Design of Monopulse Antenna Difference Patterns with Low Sidelobes*

By E. T. BAYLISS

(Manuscript received August 9, 1967)

The flexibility of modern monopulse radar antenna systems makes possible the independent optimization of sum and difference patterns. The two parameter difference pattern, developed here for the circular aperature antenna, is designed to have nearly equal sidelobes similar to those of the Taylor sum pattern. The difference pattern is asymptotic to a model difference pattern which has the greatest slope (angle sensitivity) for a given sidelobe level. The model function is unrealizable because it has uniform sidelobes which are infinite in extent. The two parameter difference pattern is realizable and is expressed in a Fourier–Bessel series of N terms in a manner similar to Taylor's treatment of the sum pattern. The other parameter, A, controls sidelobe level.

Comprehensive tables of the Fourier–Bessel coefficients are given for both the circular aperture series and the difference pattern series. Directivity and angle sensitivity are investigated and found to have maximum values that decrease as sidelobe level decreases. The monopulse system performance using the asymptotic difference pattern and the Taylor sum pattern compares favorably with a maximum likelihood angle estimation system. Development of a line source difference pattern is presented in the appendix.

I. INTRODUCTION

Monopulse radar systems have, in recent years, achieved a high degree of flexibility in their antenna patterns. This flexibility is the result of development of multihorn feed structures and array antennas. It now appears feasible to optimize independently the sum and difference patterns of the monopulse system. A good deal of work has been done to improve the sidelobe performance for sum beam pat-

terns.[1] However, less attention has been paid to improving the angle sensitivity and sidelobe performance of the circular aperture difference pattern.

The objective of this investigation was to develop a difference pattern which possesses characteristics that are compatible with those of the Taylor sum pattern. Specifically, the goal was to obtain the maximum angle sensitivity commensurate with a given sidelobe level. Low sidelobes are desirable in both sum and difference patterns for the suppression of near-target clutter, ground clutter, and jammers. Requiring large angle sensitivity and low sidelobes for the difference pattern is analogous to requiring a narrow beamwidth and low sidelobes in the case of the sum beam. The pattern that meets these requirements must be produced by a reasonably well behaved aperture illumination.

This paper solves the problem of generating difference patterns by using a technique that parallels Taylor's approach to the sum pattern design. The problem is first detailed in terms of making good angle estimates. It is attacked by applying a general synthesis technique to the approximation of a model difference pattern. Finally, the resulting asymptotic difference pattern is examined for angle sensitivity. Pertinent design information is presented.

II. THE PROBLEM—ANGULAR ESTIMATION IN NOISE USING ANTENNA DIFFERENCE PATTERNS

A monopulse system can make a maximum likelihood angle estimate[2] under one of the following assumptions:

(*i*) The primary source of noise is spatially and temporally uncorrelated noise from the radiation field

(*ii*) The primary source of noise is thermal noise which is independent in the sum and difference channels.

The angle estimate is made by correlating the sum and difference channel outputs. The sum and difference patterns required to make the maximum likelihood estimate unfortunately have quite high sidelobes (for example, the difference pattern first sidelobe is only 14.5 dB below the sum beam maximum). For applications where clutter or active noise sources are a problem, such high sidelobes are clearly unacceptable. Techniques used to suppress sidelobes can be expected to reduce the angle sensitivity. (This tradeoff is examined in Section IV.) Thus, the problem is to suppress antenna sidelobes in *both* the

difference and sum patterns without severely degrading the angle sensitivity of the system.

The objective of this paper is to provide a unified approach to difference pattern design for the monopulse system. Specifically, the objectives are to:

(*i*) Design a difference pattern with equal sidelobes, similar to sidelobes of Taylor sum pattern.

(*ii*) Solve the practical problem of generating the aperture function for the circular aperture.

(*iii*) Balance sidelobe level and angle sensitivity to get the best angle sensitivity for a given sidelobe level.

(*iv*) Compute and tabulate such design parameters as angle sensitivity, directivity, sidelobe level and, of course, the aperture generating functions.

III. THE SOLUTION—AN ASYMPTOTIC PATTERN FUNCTION WITH UNIFORM SIDELOBE LEVEL

3.1 *Aperture and Pattern Functions*

The aperture screen concept is very useful in the analysis of planar antennas. It is well known that from the tangential **E** and **H** fields on a surface enclosing a source one can, in principle, calculate the radiated fields. If the enclosing surface is an infinite plane, then some useful simplifications can be made. The equivalence principle and image theory[3] can be used to determine the field in the source-free half-space ($z > 0$) from its tangential components on the plane ($z = 0$ in Fig. 1). For this special case the E-field can be determined solely from the E-field on the plane.[3]

Plonsey[4] has pointed out that it is possible to describe the field in the Fraunhofer region for *all* $\theta < \pi/2$ where the usual Kirchhoff scalar diffraction approximation[5] is good only for small θ.

The aperture and pattern expression can be put in standard form by making the following change of variables:

$$u = \frac{2a}{\lambda} \sin \theta \quad \text{and} \quad p = \frac{\pi}{a} \rho \tag{1}$$

where u is the angle variable measured in standard beamwidths, p is the normalized aperture variable and a is the radius of the antenna, (Fig. 1). It is of interest to consider the case where the vector field
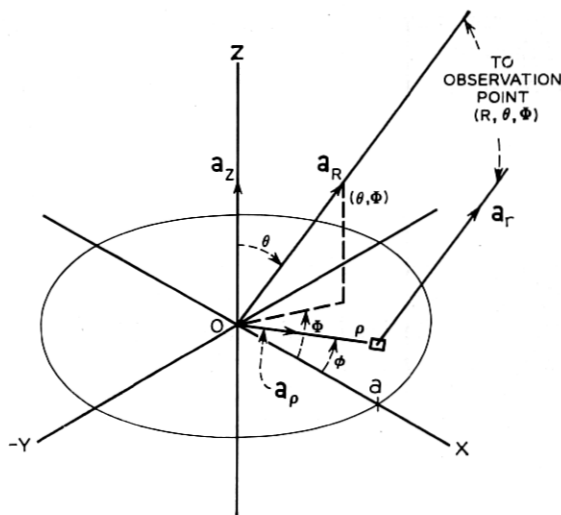
Fig. 1 — Aperture geometry.

in the aperture is factorable:

$$
\mathbf{E}\left[p, \frac{\pi}{2}, \varphi\right] = \begin{cases} (\mathbf{a}_x + \gamma \mathbf{a}_v)g(p, \varphi); & p \leqq \pi \\ 0; & \text{elsewhere} \end{cases} \tag{2}
$$

where γ is a complex constant, $\mathbf{a}_i$ is a unit vector and $g(p, \varphi)$ is the complex scalar aperture function. Notice for linear polarization, $\gamma = 0$, and for circular polarization, $\gamma = \pm j$. Under the above assumptions and with the usual Fraunhofer approximations (that is, $\rho \ll R$, $1 \ll kR$)

$$
\mathbf{E}(R, \theta, \Phi) = \frac{-je^{-jkR}}{kR} \{\mathbf{a}_R \times [\mathbf{a}_z \times (\mathbf{a}_x + \gamma \mathbf{a}_v)]\} \left(\frac{2a}{\lambda}\right)^2 F(u, \Phi); \quad \theta < \frac{\pi}{2} \tag{3}
$$

where

$$
F(u, \Phi) = \frac{1}{2\pi} \int_0^{2\pi} d\varphi \int_0^{\pi} g(p, \varphi) \exp\left[jup \cos(\Phi - \varphi)\right]p \, dp. \tag{4}
$$

The pattern function, $F(u, \Phi)$, which is the Fourier-Hankel transform of the aperture function, $g(p, \varphi)$, will be the starting point for the next section.

3.2 *Synthesis Method for Circular Apertures*

The procedure for synthesizing an arbitrary pattern function with a circular aperture is an application of Woodward's technique to the circular aperture synthesis problem.[6]

The aperture function can be represented as a Fourier-Bessel series

$$g(p, \varphi) = \sum_{k=-\infty}^{\infty} \sum_{l=0}^{\infty} a_{kl} e^{jk\varphi} J_k(\mu_{kl} p); \qquad p \leqq \pi. \tag{5}$$

This series has orthogonality and completeness properties for appropriately chosen μ_{kl}. It converges in the mean to an arbitrary aperture function, $\hat{g}(p, \varphi)$, when the complex coefficients, a_{kl}, are found by taking the inner product of the function with each orthogonal function.

The Sturm–Liouville boundary conditions give rise to the eigenvalues for the angular and radial eigenfunctions:

(*i*) The angular eigenfunctions must satisfy periodic boundary conditions. Thus their eigenvalues are the integers k.

(*ii*) The radial eigenfunctions must satisfy one of two cases:

1. $J_k(\mu_{kl}\pi) = 0$; $\mu_{kl} > 0$, $k \geqq 0$, $l = 0, 1, 2, \cdots$.
2. $cJ_k(\mu_{kl}\pi) + \mu_{kl}\pi J_k'(\mu_{kl}\pi) = 0$; $c \geqq 0$, $c^2 + k^2 > 0$, $\mu_{kl} > 0$ for $l = 0, 1, 2, \cdots$ except when $c = k = 0$ then $\mu_{00} = 0$.

The selection of case 1 or 2 and the constant c determine the set of positive distinct eigenvalues to be used in the radial eigenfunctions of (5).

The aperture function expansion that allows nonzero boundary values (case 2) is to be preferred in the expansion of equal sidelobe patterns because:

(*i*) As Taylor[1] has shown, the slowest far sidelobe decay rate results from nonzero boundary values.

(*ii*) The "central region" ($| u | < \mu_{kN}$) zeros are confined to a smaller region. This means that better sidelobe control can be obtained in the central region for a given main-beam performance and a fixed number of terms, N.

Thus, choosing case 2, let $c = 0$. The synthesis of a difference pattern allows simplification of (5) because of the symmetry required. The difference pattern requires an antiphase aperture [one sign reversal, $\hat{F}(u, \Phi) = -\hat{F}(u, \Phi + \pi)$], thus only first order Fourier components are required ($k = \pm 1$). Thus choosing $k = 1$, the boundary conditions reduce to*

---

* Primes denote differentiation with respect to the argument.

$$J_1'(u_l\pi) = 0 \qquad l = 0, 1, \cdots \tag{6}$$

where the k subscript on μ_{kl} has been dropped. See Table I for values of μ_l .

To further simplify the choice of coefficients, let the difference axis be $\varphi = \Phi = 0$. This requires setting $a_{1l} = -a_{-1l} = B_l/2$ and gives

$$\tilde{g}(p, \varphi) = \cos\varphi \sum_{l=0}^{N-1} B_l J_1(\mu_l p); \qquad p \leqq \pi. \tag{7}$$

The N-term approximation to the required function g or $\hat{F}$ is designated by a tilde $\tilde{g}$ or $\tilde{F}$. The pattern function expansion corresponding to $\tilde{g}(p, \varphi)$ in equation (7), that is, transformed by (4), is

$$\tilde{F}(u, \Phi) = j \cos\Phi \sum_{l=0}^{N-1} B_l J_1(\mu_l\pi) \frac{u J_1'(\pi u)}{\mu_l^2 - u^2}. \tag{8}$$

The terms of (8)

$$J_1(\mu_i\pi) \frac{u J_1'(\pi u)}{\mu_i^2 - u^2} ,$$

are shown in Figure 2.

The pattern function series (8) has the important "sampling" property which many approximation techniques use. If (8) is set equal to the required pattern function, $\hat{F}(u, \Phi)$, at the sample point $(\mu_m , 0)$ then the mth coefficient, B_m , can be evaluated because all other terms of (8) are zero there. Equation (8) is evaluated at $(\mu_m , 0)$ by applying L'Hôspital's rule, substituting Bessel's equation and the boundary value (6) to obtain

$$\tilde{F}(\mu_m , 0) = B_m j \frac{\pi^2}{2} J_1^2(\mu_m\pi)[1 - (\pi\mu_m)^{-2}]. \tag{9}$$

TABLE I — BESSEL FUNCTION ZEROS, $J_1'(\mu_l\pi) = 0$

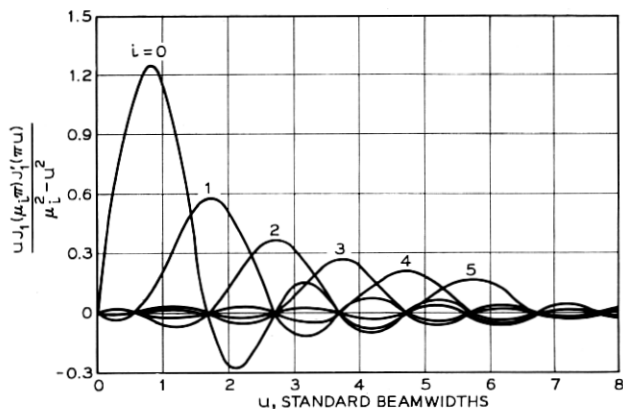| l	μ_l	l	μ_l	l	μ_l	l	μ_l
0	0.5860670	5	5.7345205	10	10.7417435	15	15.7443679
1	1.6970509	6	6.7368281	11	11.7424475	16	16.7447044
2	2.7171939	7	7.7385356	12	12.7430408	17	17.7450030
3	3.7261370	8	8.7398505	13	13.7435477	18	18.7452697
4	4.7312271	9	9.7408945	14	14.7439856	19	19.7455093

Fig. 2 — Bessel series pattern function terms.

Now setting (9) equal to $\hat{F}(u, \Phi)$ at the sample points, the coefficients of (8) are evaluated

$$B_m = \hat{F}(\mu_m, 0) \frac{2}{j\pi^2} J_1^{-2}(\mu_m \pi)[1 - (\pi\mu_m)^{-2}]^{-1};$$

$$m = 0, 1, 2, \cdots, N - 1. \qquad (10)$$

In Section 3.4 (10) is used to evaluate the coefficients from sample points on the model function, F_M, and thus determine the aperture function (7) and pattern function (8).

3.3 Construction of a Model Pattern Function

The previous section provides a method of expanding any realizable pattern function. In this section a model difference pattern function is developed. It will serve as a model for the construction of the asymptotic difference pattern in the next section. Thus its role is analogous to Taylor's "ideal function."[1]

The main characteristic desired in a model function is maximum angular sensitivity for a given sidelobe level. It has been shown[7] for an array that the pattern function that produces the greatest angular sensitivity with a given sidelobe level must also have sidelobes of *equal* height. This theorem is analogous to that proved by Dolph for the sum pattern.[8]

Two important differences occur when the above result for an array is extended to the case of the continuous aperture:

(*i*) The pattern function has maximum slope for a given sidelobe level (not maximum sensitivity).

(*ii*) The pattern function is not a realizable antenna pattern.

These two characteristics result from requiring the difference pattern to have sidelobes of equal height. These equal sidelobes now are infinite in extent (for all u). Any pattern function whose sidelobes do not decay at least as $u^{-3/2}$ is not realizable because it requires an unbounded aperture function. Because the function is unrealizable its angular sensitivity is undefined. Nevertheless it does have the maximum slope for a given sidelobe level and will serve as a model function for synthesis of a realizable asymptotic difference pattern in Section 3.4.

Thus, the main characteristics of the model function are:

(*i*) Maximum slope at the origin for a given peak-to-sidelobe ratio.
(*ii*) Sidelobes of uniform magnitude and infinite in extent.

Price and Hyneman pointed out that an exact functional form for such a function is not known. What follows is a method for constructing a very close approximation to the equal sidelobe difference pattern function.

The ideal sum pattern used by Taylor[1] is of the form

$$F_\Sigma(u) = \cos \pi \sqrt{u^2 - A^2} \tag{11}$$

where A is a parameter that determines the sidelobe level. This function has equal sidelobes that are infinite in extent. Taking the derivative of the ideal sum pattern a difference pattern is obtained.

$$F_\Delta(u) = \pi(u^2 - A^2)^{-1/2} u \sin \pi(u^2 - A^2)^{+1/2}. \tag{12}$$

The first few sidelobes of this function are not of equal height as can be seen from the dashed curves in Figure 3. However, it is possible to modify the first few sidelobes of the above function so that they are equal to the asymptotic sidelobe level. The zeros of the above function are given by

$$z_n = \begin{cases} 0; & n = 0 \\ \pm(A^2 + n^2)^{\frac{1}{2}}; & n = 1, 2, 3, \cdots \end{cases} \tag{13}$$

A model difference function can be constructed by moving the first T zeros on either side of the origin so that the sidelobes are made
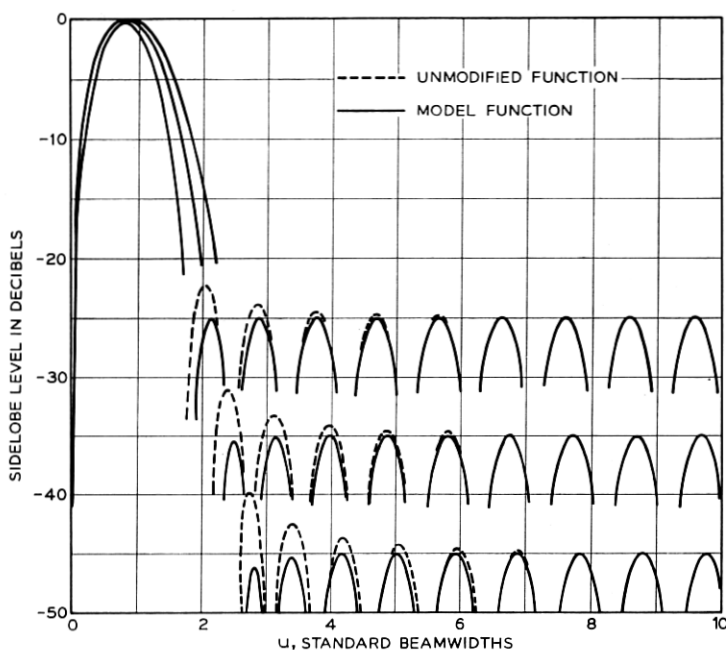
Fig. 3 — Model difference pattern compared with unmodified function for sidelobe levels of 25, 35, and 45 dB.

equal. The model difference function is given by

$$F_M(u) = F_\Delta(u) \prod_{n=1}^{T} \frac{\xi_n^2 - u^2}{z_n^2 - u^2} \qquad (14)$$

where the zeros, z_n, are moved to ξ_n. The location of the new zero ξ_n which make the sidelobes equal can be found by an iterative procedure.[9] Very good results were obtained by moving only the first four zeros on either side of the origin. The constructed model functions are shown in Figure 3 as solid curves.

To expedite future computations the sidelobe parameter A and the zeros were fitted as polynomial functions of the sidelobe level in dB. Fourth degree polynomials were fitted to values of A, ξ_n, and the location of the difference peak, p_0, that were obtained from the iterative computation. Curves of the parameters along with their polynomial coefficients can be found in Figure 4.

The use of fitted polynomials inevitably leads to errors in the results. The effect of these errors is more pronounced in the low side-
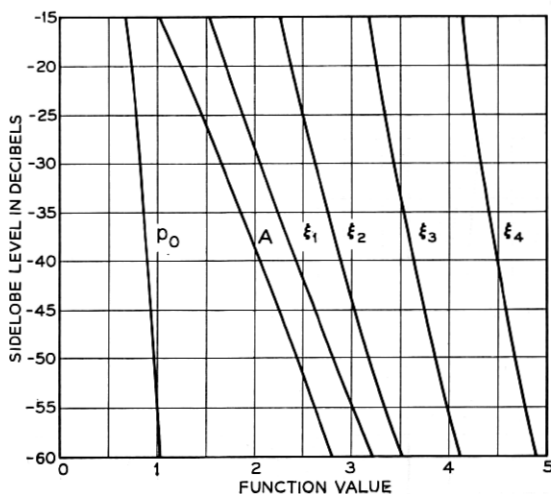
Fig. 4 — Model difference pattern parameters.

Polynomial Name	Polynomial Coefficients				
	C_0	C_1	C_2	C_3	C_4
A	0.30387530	-0.05042922	-0.00027989	-0.00000343	-0.00000002
ξ_1	0.98583020	-0.03338850	0.00014064	0.00000190	0.00000001
ξ_2	2.00337487	-0.01141548	0.00041590	0.00000373	0.00000001
ξ_3	3.00636321	-0.00683394	0.00029281	0.00000161	0.00000000
ξ_4	4.00518423	-0.00501795	0.00021735	0.00000088	0.00000000
p_0	0.47972120	-0.01456692	-0.00018739	-0.00000218	-0.00000001

lobe pattern. For example, notice the depressed first sidelobe in the -45 dB pattern of Figure 3 (and later in Figure 8). If good fidelity is desired for low sidelobe patterns it is advisable to use the calculated zeros directly and avoid use of the polynomials.

3.4 *Synthesis of Asymptotic Difference Patterns*

Now the problem of approximating the model function using the synthesis method described in Section 3.2 is considered. In this section an asymptotic form of the model function is developed. The asymptotic form is expressed in terms of the Fourier-Bessel series.

In Section 3.3 the model function for the ideal difference pattern F_M is generated in equations (12) and (14). The outstanding feature of this model function is its equal sidelobes. F_M is an entire function

of u and is completely described by its zeros,

$$Z_n = \begin{cases} 0; & n = 0 \\ \pm\xi_n; & n = 1, \cdots, T. \\ \pm(A^2 + n^2)^{\frac{1}{2}}; & n = T + 1, \cdots \end{cases} \qquad (15)$$

For large $|u|$ the zeros approach $\pm n$ asymptotically. The model function is not realizable because it does not have decaying sidelobes (nonfinite energy).

The steps in constructing the asymptotic difference pattern are illustrated in Figure 5. The behavior of the model function in the far sidelobe region is changed so that it conforms to the asymptotic behavior of a realizable pattern function with decaying sidelobes. To do this, the zeros, Z_n, of F_M for all $n \geq N$ are moved to μ_n. These new far sidelobe zeros are zeros of the truncated pattern function series (8). This series must represent a realizable pattern function.

These zeros also satisfy (6). By changing only the far sidelobe zeros we have retained the essential model function characteristics in the central region. This central region behavior is embodied in the central zeros, Z_n for $n < N$. The Nth zero pair of the model function, $\pm Z_N$, and the Nth zero pair of the realizable function, $\pm\mu_N$, do not coincide.
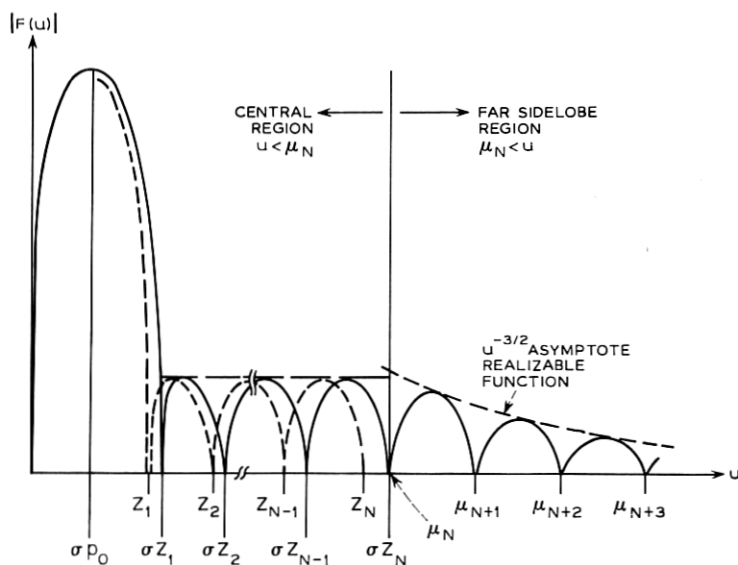

Fig. 5 — Construction of asymptotic difference pattern.

Usually, the distance between Z_{N-1} and μ_N is somewhat greater than one. Such a situation will give rise to a rather large sidelobe at the transition between central region and far sidelobe region.

To eliminate this high transition sidelobe the zeros of the central region will be dilated by a factor σ which makes Z_N and μ_N coincide

$$\sigma = \frac{\mu_N}{Z_N}. \tag{16}$$

For sufficiently large N, σ will always be greater than one.
The steps illustrated by Figure 5 are:

(*i*) A realizable pattern function with decaying sidelobes replaces the model function in the far sidelobe region.

(*ii*) The model function (dashed curve) is dilated so that the zero (σZ_N) coincides with the first zero of the far sidelobe region at $u = \mu_N$.

The asymptotic form of the model function is essentially complete. It can be expressed as a cononical product of its zeros

$$F_a(u, \Phi) = Cu\pi \cos \Phi \prod_{n=1}^{N-1} \left[1 - \left(\frac{u}{\sigma Z_n}\right)^2 \right] \prod_{n=N}^{\infty} \left[1 - \left(\frac{u}{\mu_n}\right)^2 \right] \tag{17}$$

where C is a constant. The second product term must be reduced to closed functional form for this expression to have any practical value. The zeros in the second product of (17) satisfy $J_1'(\mu_n\pi) = 0$. Thus the second product term in (17) in closed form is equal to the first term of (8) with all zeros removed for $|u| < \mu_N$.

$$\prod_{n=N}^{\infty} \left\{ 1 - \left(\frac{u}{\mu_n}\right)^2 \right\} = [2J_1'(u\pi)] \left\{ \prod_{l=0}^{N-1} 1 - \left(\frac{u}{\mu_l}\right)^2 \right\}^{-1}. \tag{18}$$

Combining (17) and (18)

$$F_a(u, \Phi) = C (\cos \Phi) 2\pi u J_1'(u\pi) \frac{\displaystyle\prod_{n=1}^{N-1} \left[1 - \left(\frac{u}{\sigma Z_n}\right)^2 \right]}{\displaystyle\prod_{l=0}^{N-1} \left[1 - \left(\frac{u}{\mu_l}\right)^2 \right]}. \tag{19}$$

$F_a(u, \Phi)$ is a realizable asymptotic difference pattern. It is nearly equal to the model function in the central region (that is, $|u| < \mu_N$). In fact, as the size of the central region increases without bound, the asymptotic function approaches the model function

$$\lim_{N \to \infty} F_a(u, \Phi) = F_M(u, \Phi). \tag{20}$$

The limit can be deduced from (17) by noting that asymptotic behavior of μ_N (6) gives

$$\sigma = \frac{\mu_N}{[A^2 + N^2]^{\frac{1}{2}}} \approx 1 + \frac{\frac{3}{4}}{N}, \qquad 1 < T \ll N. \qquad (21)$$

Now as N is increased $\sigma \to 1$. Thus as N goes to infinity (and $\sigma \to 1$) the second product term (17) disappears and only the first remains. The first product term (with $\sigma = 1$) is exactly equal to the model function. Thus $F_a(u, \Phi)$ is truly asymptotic to $F_M(u, \Phi)$.

The asymptotic function (19) is expressed as a Fourier–Bessel series using equation (10) to evaluate the coefficients. First evaluate $F_a(u, \Phi)$ at the sample points $(\mu_m, 0)$

$$\hat{F}(\mu_m, 0) = F_a(\mu_m, 0) = C2\pi\mu_m \frac{\prod\limits_{n=1}^{N-1}\left[1 - \left(\frac{\mu_m}{\sigma Z_n}\right)^2\right]}{\prod\limits_{\substack{l=0 \\ l \neq m}}^{N-1}\left[1 - \left(\frac{\mu_m}{\mu_l}\right)^2\right]} \operatorname*{Lim}_{u \to \mu_m} \frac{J_1'(u\pi)}{\left[1 - \left(\frac{u}{\mu_m}\right)^2\right]}$$

$$m = 0, 1, \cdots, N - 1. \qquad (22)$$

Evaluating the limit and substituting Bessel's equation yields

$$F_a(\mu_m, 0) = C(\pi\mu_m)^2[1 - (\pi\mu_m)^{-2}]J_1(\mu_m\pi) \frac{\prod\limits_{n=1}^{N-1}\left[1 - \left(\frac{\mu_m}{\sigma Z_n}\right)^2\right]}{\prod\limits_{\substack{l=0 \\ l \neq m}}^{N-1}\left[1 - \left(\frac{\mu_m}{\mu_l}\right)^2\right]}$$

$$m = 0, 1, \cdots, N - 1. \qquad (23)$$

Notice also that because of the construction of the asymptotic function $F_a(\mu_m, 0) = 0$ for $m \geq N$. Finally the coefficients from (10) are:

$$B_m = \begin{cases} \dfrac{-Cj2\mu_m^2}{J_1(\mu_m\pi)} \dfrac{\prod\limits_{n=1}^{N-1}\left[1 - \left(\frac{\mu_m}{\sigma Z_n}\right)^2\right]}{\prod\limits_{\substack{l=0 \\ l \neq m}}^{N-1}\left[1 - \left(\frac{\mu_m}{\mu_l}\right)^2\right]} ; & m = 0, 1, \cdots, N - 1 \\[4ex] 0 & ; \qquad m = N, N + 1, \cdots \end{cases} \qquad (24)$$

where μ_m is given by (6), Z_n by (15) and σ by (16). The constant C is evaluated so that the peak of the asymptotic difference pattern is unity, that is, $F_a(\sigma p_0, 0) = 1$.

The pattern function expansion (8) is identically *equal* to the asymp-

totic difference pattern, $F_a(u, \Phi)$, because only the first N coefficients (24) are nonzero, thus the series terminates. Furthermore, the expansion (7) is equal to the aperture function of the asymptotic difference pattern. Thus equations (24), (8), and (7) define the solution to the problem of finding a difference pattern compatible with the Taylor sum pattern. (A similar function is developed for the line source in the appendix.) This realizable two-parameter difference pattern is asymptotic to the model function. The parameter A controls the sidelobe level of the pattern. The parameter N controls the size of the central region; hence, it controls the degree of approximation to the model function.

IV. THE RESULT—DESIGN DATA AND PATTERN CHARACTERISTICS

4.1 Pattern and Aperture Functions

The usefulness of a pattern function is determined largely by the availability of design data about the pattern. Coefficients B_l were calculated in equation (24) for sidelobe levels from -17.5 dB to -45 dB at 2.5 dB intervals and for $N = 3$ to 30. Coefficients for selected values of N appear in Tables II and III. The coefficients are normalized to make the difference pattern peak equal to unity.

The coefficients are used, in equation (7), to generate the aperture function with $\varphi = 0$ (Figures 6 and 7). Some observations can be made regarding the effects of the parameters on the aperture function:

TABLE II — COEFFICIENTS FOR δ_{max} PATTERNS

COEFFICIENTS N=	5	7	8	11	14	17	21	27	30	30	30	30
SLL=	−17.5	−20.0	−22.5	−25.0	−27.5	−30.0	−32.5	−35.0	−37.5	−40.0	−42.5	−45.0
B 0	0.79738	0.79422	0.78677	0.78215	0.77598	0.76878	0.76183	0.75508	0.74706	0.73851	0.73009	0.72200
B 1	0.14654	0.20764	0.30017	0.36076	0.42971	0.49981	0.56485	0.62432	0.68963	0.75578	0.81714	0.87429
B 2	0.13474	0.11727	0.06774	0.04336	0.01691	−0.00460	−0.01848	−0.02572	−0.02877	−0.02588	−0.01699	−0.00303
B 3	−0.15632	−0.18338	−0.13874	−0.12031	−0.09011	−0.06174	−0.04006	−0.02421	−0.01019	0.00022	0.00651	0.00973
B 4	0.09650	0.18907	0.16174	0.16100	0.13248	0.10080	0.07503	0.05502	0.03628	0.02125	0.01079	0.00375
B 5		−0.15105	−0.15245	−0.18152	−0.16116	−0.12935	−0.10140	−0.07855	−0.05604	−0.03749	−0.02412	−0.01464
B 6		0.08042	0.11498	0.18236	0.17722	0.14914	0.12134	0.09701	0.07139	0.04984	0.03410	0.02272
B 7			−0.05983	−0.16641	−0.18258	−0.16223	−0.13703	−0.11286	−0.08443	−0.06016	−0.04233	−0.02932
B 8				0.13589	0.17757	0.16881	0.14884	0.12604	0.09575	0.06900	0.04929	0.03485
B 9				−0.09434	−0.16273	−0.16888	−0.15679	−0.13730	−0.10558	−0.07661	−0.05523	−0.03952
B10				0.04678	0.13912	0.16253	0.16080	0.14645	0.11398	0.08307	0.06024	0.04344
B11					−0.10843	−0.15009	−0.16080	−0.15342	−0.12094	−0.08841	−0.06437	−0.04667
B12					0.07294	0.13214	0.15681	0.15811	0.12642	0.09261	0.06762	0.04921
B13					−0.03554	−0.10956	−0.14893	−0.16046	−0.13036	−0.09565	−0.06999	−0.05107
B14						0.08348	0.13742	0.16040	0.13271	0.09750	0.07146	0.05226
B15						−0.05531	−0.12261	−0.15794	−0.13343	−0.09813	−0.07202	−0.05276
B16						0.02676	0.10500	0.15309	0.13250	0.09753	0.07167	0.05258
B17							−0.08518	−0.14594	−0.12993	−0.09572	−0.07040	−0.05172
B18							0.06387	0.13661	0.12575	0.09270	0.06825	0.05019
B19							−0.04188	−0.12528	−0.12000	−0.08853	−0.06524	−0.04803
B20							0.02018	0.11216	0.11275	0.08324	0.06140	0.04525
B21								−0.09749	−0.10409	−0.07691	−0.05677	−0.04188
B22								0.08144	0.09395	0.06947	0.05133	0.03790
B23								−0.07256	−0.08964	−0.06646	−0.04925	−0.03649
B24								0.04915	0.07314	0.05417	0.04010	0.02987
B25								−0.03185	−0.06044	−0.04481	−0.03320	−0.02460
B26								0.01530	0.04762	0.03534	0.02621	0.01944
B27									−0.03472	−0.02579	−0.01915	−0.01422
B28									0.02199	0.01635	0.01215	0.00903
B29									−0.00976	−0.00725	−0.00539	−0.00400

TABLE III — COEFFICIENTS FOR DIFFERENCE PATTERNS

N = 5

COEFFICIENTS \ SLL=	−17.5	−20.0	−22.5	−25.0	−27.5	−30.0	−32.5	−35.0	−37.5	−40.0	−42.5	−45.0
B 0	0.79738	0.78751	0.77806	0.76893	0.76033	0.75219	0.74458	0.73722	0.73042	0.72392	0.71792	0.71213
B 1	0.14654	0.26831	0.37445	0.46772	0.55036	0.62400	0.69001	0.74921	0.80278	0.85116	0.89522	0.93516
B 2	0.13474	0.06408	0.01520	−0.01692	−0.03613	−0.04535	−0.04690	−0.04252	−0.03364	−0.02137	−0.00658	0.01005
B 3	−0.15632	−0.09756	−0.05612	−0.02743	−0.00808	0.00445	0.01209	0.01623	0.01796	0.01804	0.01706	0.01544
B 4	0.09650	0.06431	0.04125	0.02488	0.01343	0.00556	0.00029	−0.00311	−0.00517	−0.00631	−0.00680	−0.00686

N = 10

COEFFICIENTS \ SLL=	−17.5	−20.0	−22.5	−25.0	−27.5	−30.0	−32.5	−35.0	−37.5	−40.0	−42.5	−45.0
B 0	0.81073	0.80063	0.79056	0.78064	0.77095	0.76154	0.75248	0.74367	0.73523	0.72715	0.71935	0.71189
B 1	0.02204	0.15201	0.26817	0.37274	0.46739	0.55343	0.63195	0.70372	0.76955	0.83004	0.88566	0.93694
B 2	0.26549	0.16480	0.09021	0.03653	−0.00030	−0.02345	−0.03549	−0.03846	−0.03404	−0.02362	−0.00834	0.01085
B 3	−0.37699	−0.25968	−0.17324	−0.11027	−0.06513	−0.03349	−0.01200	0.00191	0.01023	0.01451	0.01596	0.01549
B 4	0.43812	0.30936	0.21485	0.14597	0.09622	0.06071	0.03576	0.01858	0.00708	−0.00031	−0.00478	−0.00721
B 5	−0.45439	−0.32444	−0.22918	−0.15972	−0.10940	−0.07324	−0.04751	−0.02942	−0.01690	−0.00841	−0.00281	0.00074
B 6	0.42252	0.30349	0.21625	0.15259	0.10637	0.07303	0.04915	0.03219	0.02027	0.01201	0.00638	0.00262
B 7	−0.34848	−0.25158	−0.18048	−0.12849	−0.09065	−0.06323	−0.04349	−0.02935	−0.01932	−0.01227	−0.00737	−0.00401
B 8	0.24219	0.17579	0.12694	0.09111	0.06493	0.04586	0.03205	0.02208	0.01495	0.00987	0.00629	0.00380
B 9	−0.11903	−0.08696	−0.06326	−0.04580	−0.03297	−0.02356	−0.01670	−0.01171	−0.00810	−0.00550	−0.00364	−0.00232

first, when N is fixed (Figure 6), one sees that increasing the sidelobe level decreases the peak but increases the edge illumination. Conversely, when the sidelobe level is held constant (Figure 7), the effect of increasing N reduces the peak only slightly but increases the edge illumination tremendously. One of the prominent characteristics of this type of pattern synthesis is that the edge illumination increases as N increases.
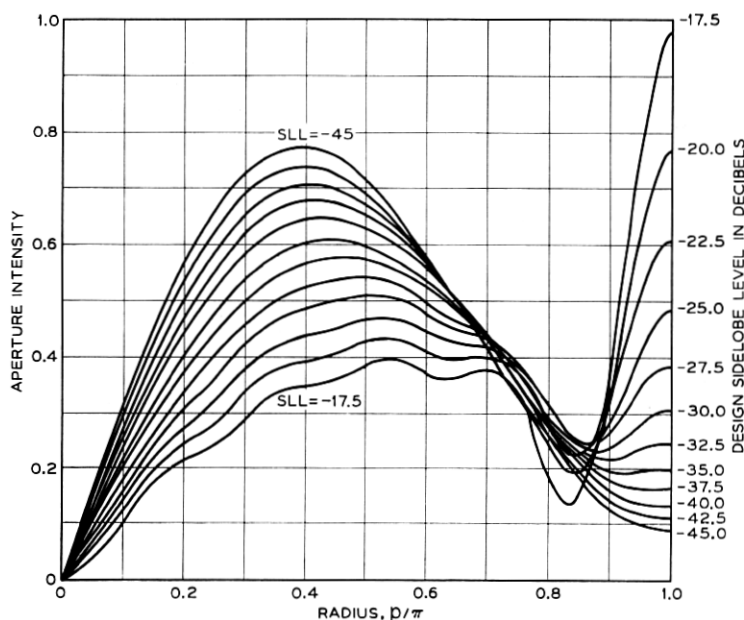
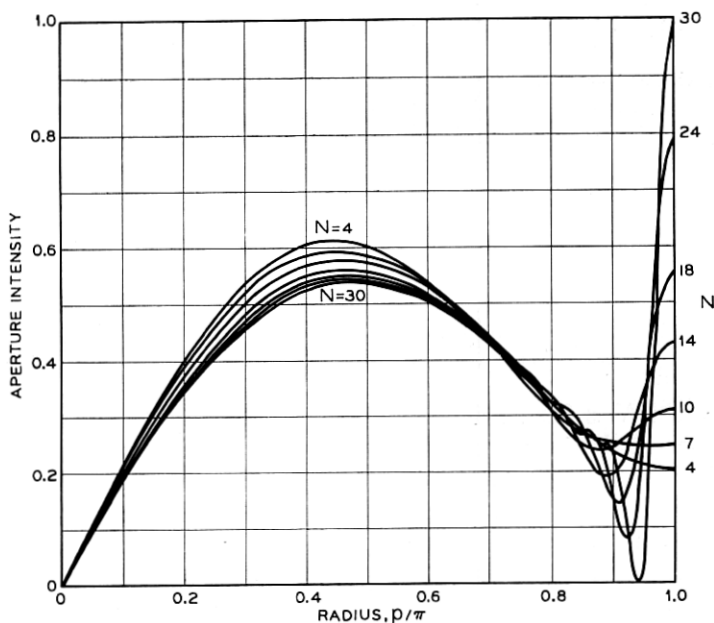Fig. 6 — Circular aperture functions for $N = 10$.

Fig. 7 — Circular aperture functions for −30 dB sidelobe level.

The pattern functions exhibit a more straightforward dependence on the two parameters. The sidelobe envelopes are plotted in Figure 8 and 9 that correspond to the aperture functions in Figures 6 and 7. Only the envelope is plotted with a ○ to mark the sidelobe peak. Obviously the sidelobe parameter controls the maximum sidelobe level. The suppression of the first few sidelobes for very low sidelobe levels (Figure 8) is caused by using too small an N. When nondecreasing sidelobes are encountered the pattern is in a nonasymptotic region indicating that there are not enough terms in the series.

The effect of changing N can best be seen by keeping the sidelobe level fixed (Figure 9). As N is increased the sidelobes become more nearly equal as well as increasing the region affected. If we examine the sidelobe more closely we see that an inflection occurs at about $u = N$. The inflection results from the transition between the central region where the zeros have been modified and the far sidelobe region where the natural decay envelope is $u^{-3/2}$ (Figure 10).

The asymptotic behavior of a given pattern function for large u can be examined in a manner similar to Taylor's[1], giving the asymptotic

form of the pattern function as

$$F(u, \Phi) \sim \frac{(2\pi)^{\alpha+1}\Gamma(\alpha + 1)}{\pi\sqrt{2}\ u^{(\frac{3}{2})+\alpha}}$$

$$\cdot \frac{h(\pi, \Phi)\ \exp\left[j\pi\left(u - \frac{3}{4} - \frac{\alpha}{2}\right)\right] + h(\pi, \Phi + \pi)\ \exp\left[-j\pi\left(u - \frac{3}{4} - \frac{\alpha}{2}\right)\right]}{2}$$

$$\text{for } |u| \to \infty \quad \text{and} \quad \mathrm{Re}\ u > 0. \qquad (25)$$

The above notation follows Taylor's except that the aperture function is defined over the entire aperture not just on a line. The function
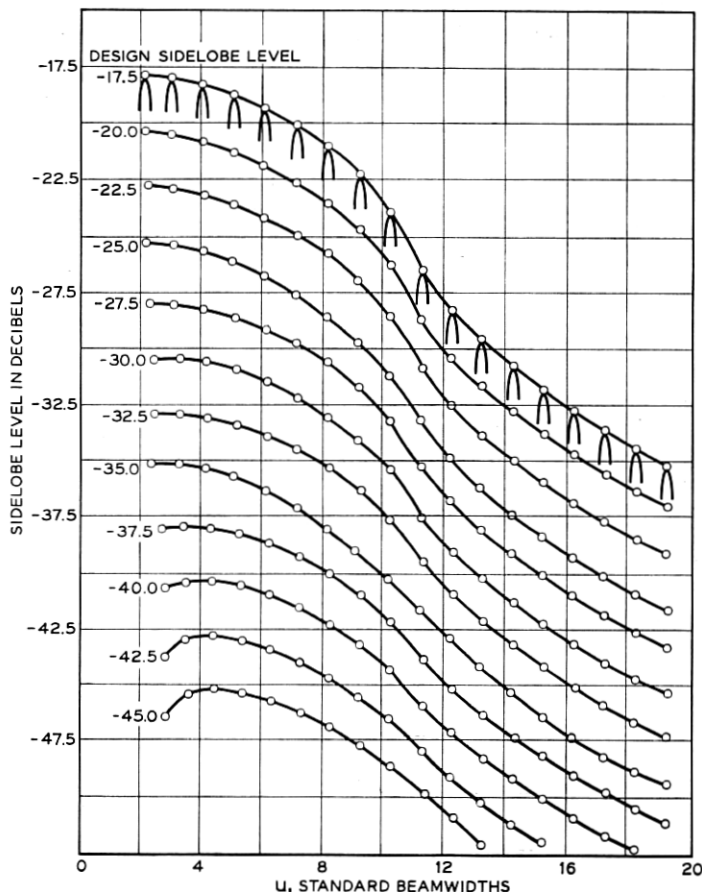
Fig. 8 — Sidelobe envelope of pattern functions for $N = 10$.

$h(p, \Phi)$ is the analytic part of the aperture function, that is, $g(p, \Phi) = h(p, \varphi)(\pi^2 - p^2)^\alpha$. For nonzero boundary values $\alpha = 0$ and $h(p, \varphi) = g(p, \varphi)$. Evaluating (25) for the difference pattern gives

$$F(u, \Phi) \sim \sqrt{2}\, g(\pi, \Phi)\, \frac{\sin \pi(u - \frac{3}{4})}{u^{\frac{3}{2}}}. \tag{26}$$

As one might expect when dealing with aperture-limited functions the asymptotic form of the pattern function depends only on the aperture function behavior at the boundary of the aperture. The asymptote in Figure 10 was computed from equation (26).

To pursue the topic of asymptotic behavior further leads to considering the superdirectivity ratio and "Q" of the antenna. A rough qualitative definition would describe the superdirectivity ratio as the ratio of total power flow through the aperture to the power that is actually radiated. The definition of Q is the ratio of energy stored in the near field (evanescent waves) to that radiated per cycle. Increasing the superdirectivity increases the reactive component of power flow (also Q) and thus increases the ohmic losses in the antenna.
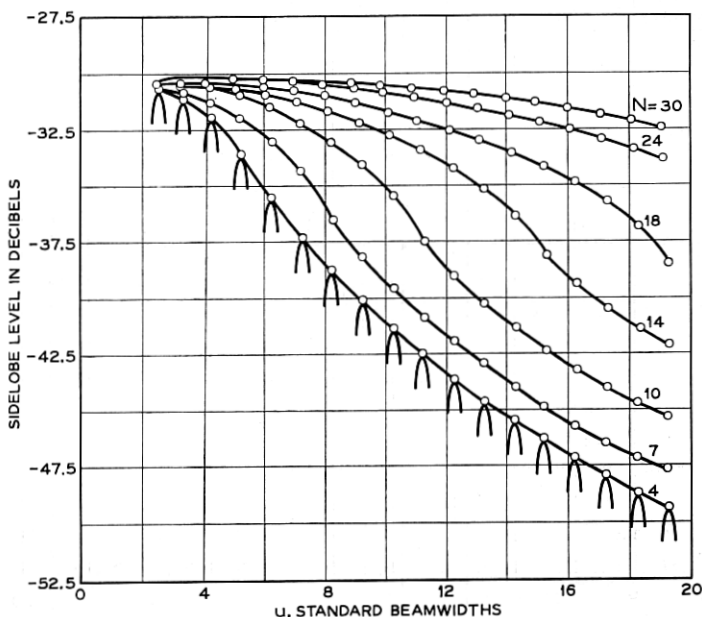

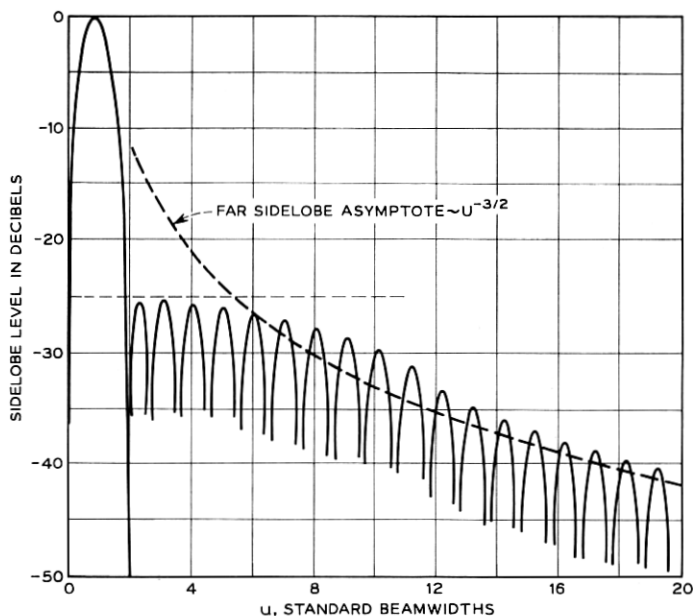Fig. 9 — Sidelobe envelope of pattern functions for -30 db sidelobe level.

Fig. 10 — Asymptotic sidelobe behavior for —25dB sidelobe level and $N = 11$.

Large superdirectivity ratios are to be avoided (expect in very small antennas) for a number of practical reasons: high ohmic losses, high error sensitivity, and narrow bandwidth. How then is superdirectivity affected by the choice of difference pattern? Superdirectivity increases as the integrated power of the pattern function in the region $u > 2a/\lambda$ increases. This means that for a given sidelobe level superdirectivity increases with N. However, for a given pattern function, superdirectivity decreases with increasing antenna diameter. Because of the undesirable effect of the reactive component, the parameter N should be chosen so that $N < 2a/\lambda$.

The asymptotic behavior of the pattern function as N is increased is best illustrated by the dilation factor, σ (Figure 11). The dilation factor decreases to one as N is increased toward infinity. In the non-asymptotic region (Figure 11) the dilation actually increases with N. Because of severe sidelobe anomalies it is best to avoid using patterns with N in the nonasymptotic region. For $N = 30$ the pattern dilation is less than 3 per cent for all sidelobe levels.
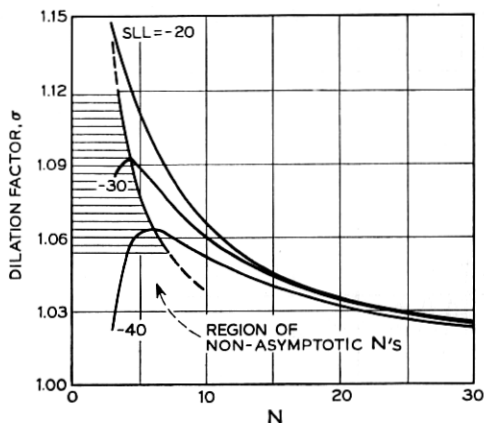
Fig. 11 — Pattern dilation factor, σ.

4.2 Pattern Characteristics

A figure of merit by which the performance of a pattern can be measured against other patterns is a great help in selecting a specific pattern. Two such figures are directivity and angular sensitivity.

The directivity function is defined so that the aperture function can be used to find the total power

$$G(u, \Phi) = \frac{4\pi^2 a^2}{\lambda^2} \frac{\frac{4}{\pi} \mid F(u, \Phi) \mid^2}{\int_0^{2\pi} d\varphi \int_0^{\pi} \mid g(p, \varphi) \mid^2 p \, dp}. \tag{27}$$

This definition is based on Silver's work,[10] and makes the following assumptions:

(i) The effect of the obliquity factor is neglected.
(ii) The antenna is large in wavelengths.
(iii) The effects of ohmic losses in the antenna are neglected.

The maximum directivity of a uniform-phase circular aperture is

$$G_0 = \frac{4\pi^2 a^2}{\lambda^2}. \tag{28}$$

The maximum directivity of a difference pattern naturally occurs at the peak of the difference beam (u_1, Φ_1) rather than at boresight.

The directivity at the pattern maximum normalized by the maxi-

mum aperture directivity is defined as the *relative directivity*, η:

$$\eta = \frac{G(u_1, \Phi_1)}{G_0} = \frac{\frac{4}{\pi} \mid F(u_1, \Phi_1) \mid^2}{\int_0^{2\pi} d\varphi \int_0^\pi \mid g(p, \Phi) \mid^2 p \, dp} \tag{29}$$

where (u_1, Φ_1) is the pattern maximum.

This quantity is similar to aperture taper efficiency. Computation of relative directivity can now be carried out for the asymptotic difference pattern by noting that the coefficients computed for Tables II and III were normalized to make $F(u_1, \Phi_1) = 1$ and that the aperture function series is orthogonal.

$$\eta = \frac{8}{\pi^4} \left\{ \sum_{l=0}^{N-1} \mid B_l \mid^2 J_1^2(\mu_l \pi)[1 - (\mu_l \pi)^{-2}] \right\}^{-1} \tag{30}$$

Relative directivity in dB (10 log η) was plotted as a function of N and sidelobe level (Figure 12). It can be seen that there is one N that gives a maximum relative directivity. The maximum is obtained when, as N increases, the power removed from the main beam by narrowing is just offset by the power added to the sidelobes by raising more sidelobes. The maximum relative directivity that can be achieved in any difference pattern (antiphase aperture) is -2.47 dB.[11]

The most important characteristic of a difference pattern is its angle sensitivity. The angle sensitivity function is defined[12] using equation (27)

$$K(u) = \frac{\partial G^{\frac{1}{2}}(u, \Phi_1)}{\partial u} \text{ volt/volt/std. BW} \tag{31}$$
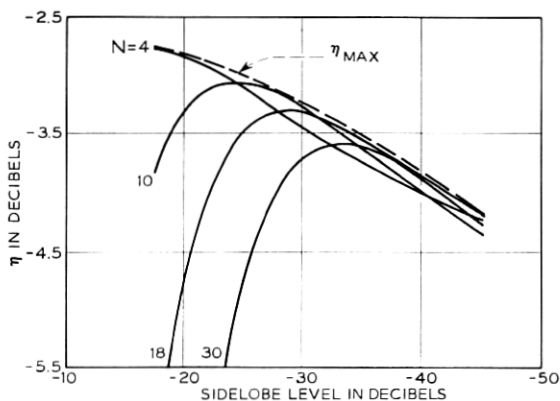

Fig. 12 — Difference pattern relative directivity, η.

where Φ_1 is the difference pattern axis. The angle sensitivity of a pattern is $K(0)$ which is the maximum value at boresight. The maximum angle sensitivity for any aperture is produced by a linear odd aperture function[12] (that is, $g = jx$). For a circular aperture its pattern function is

$$F(u, 0) = \pi \frac{J_2(\pi u)}{u}. \tag{32}$$

This pattern has -11.6 dB sidelobes and angle sensitivity

$$K_0 = \frac{\pi}{2} G_0^{\frac{1}{2}} \text{ volt/volt/std. BW.} \tag{33}$$

Again it is convenient to normalize to this maximum angular sensitivity and thus define *relative angle sensitivity* to be

$$\delta = \frac{K(0)}{K_0} = \frac{2}{\pi} \eta^{\frac{1}{2}} \left| \frac{\partial F(u, \Phi_1)}{\partial u} \right|_{u=0} \tag{34}$$

where $F(u, \Phi)$ is normalized to unity.

By evaluating the partial derivative of the difference pattern function at $u = 0$ the relative angle sensitivity is calculated as

$$\delta = \eta^{\frac{1}{2}} \sum_{l=0}^{N-1} B_l \frac{J_1(\mu_l \pi)}{\mu_l^2}. \tag{35}$$

Relative angle sensitivity in dB ($20 \log \delta$) was plotted as a function of N (Figure 13). The curves are very similar in behavior to those for
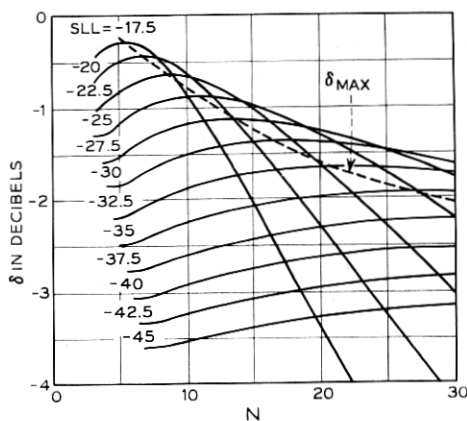

Fig. 13 — Difference pattern relative angular sensitivity, δ.

relative directivity as might be expected from equation (35). Certainly it is not unreasonable for the derivative of the directivity function at boresight to be strongly influenced by the magnitude of the peaks on either side. The dependence on sidelobe level is greater than for relative directivity. The dashed curve in Figure 13 is the maximum angle sensitivity (δ_{max}) for each sidelobe level. The pattern coefficients are given in Table II for 12 sidelobe levels with N chosen to maximize δ.

The decrease in angle sensitivity as the target moves off boresight is of interest in determining the linearity and useful angular sector of operation. The normalized angular sensitivity function, $K(u)/K_0$ is plotted for six δ_{max} patterns in Figure 14. Although the boresight sensitivity is higher for high sidelobes than for low sidelobes, it also decreases more rapidly as a function of angle.

4.3 System Performance

The sum and difference signals derived from the antenna just discussed can easily be put in a form that allows processing by any of the three types of angle detection systems.[13] The system generally used makes the angle estimate by forming a ratio of the difference to
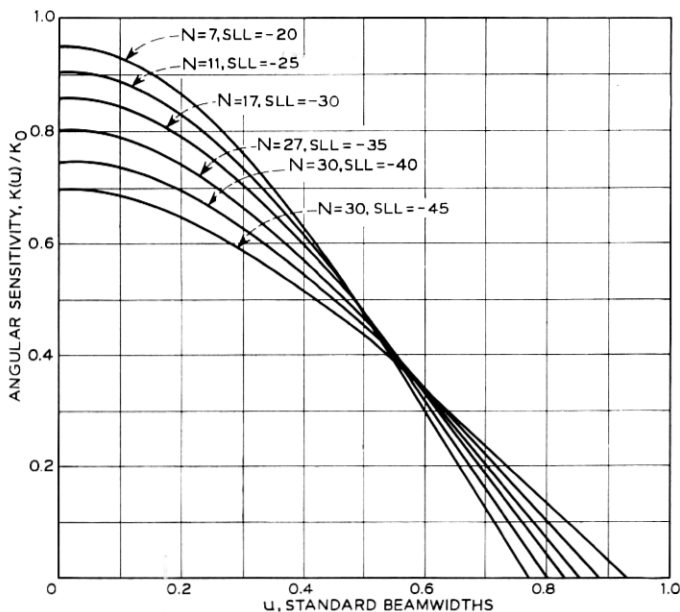

Fig. 14 — Normalized angular sensitivity function, $K(u)/K_0$.

sum signal. The statistic of this ratio was recently treated[14] with regard to maximum likelihood estimates of angle. For the high signal-to-noise case the variance of the maximum likelihood angle estimate[2, 14] is shown to be:

$$\sigma_\theta^2 = \frac{A^2}{B^2} \left(\frac{2E}{N_o}\right)^{-1} \tag{36}$$

where A and B correspond to $G_\Sigma^{\frac{1}{2}}$ and K in our notation,* E is the signal energy and N_0 is the noise power per cycle of receiver bandwidth.

Manasse had shown earlier[2] that the minimum standard deviation for the maximum likelihood angle estimate made using a circular aperture is

$$(\sigma_u)_{\text{opt}} = (\sigma_\theta)_{\text{opt}}\left(\frac{2a}{\lambda}\right) = \frac{2}{\pi}\left(\frac{2E_0}{N_0}\right)^{-\frac{1}{2}} \text{std. BW} \tag{37}$$

where $2E_0/N_0$ is the output peak signal-to-noise power ratio in a perfectly matched receiver with optimum antenna system (that is, uniform aperture function).

The effects of antenna illumination on system performance can be expressed noting that realized signal energy E is also affected by antenna sum directivity. Thus $E = E_0\eta_\Sigma L$ where L accounts for losses such as filter mismatch loss, integration loss, and transmitter and propagation losses. Then (36) expressed in standard beamwidths is

$$\sigma_u = \frac{G_\Sigma^{\frac{1}{2}}(u)}{K(u)}\left(\frac{2E_0\eta_\Sigma L}{N_0}\right)^{-\frac{1}{2}} \text{std. BW.} \tag{38}$$

Now by noting that

$$\frac{K(0)}{K_0} = \delta \quad \text{and} \quad \frac{G_\Sigma(0)}{G_0} = \eta_\Sigma ; \quad \frac{K(u)}{K(0)} \cong 1 \quad \text{and} \quad \frac{G_\Sigma(u)}{G_\Sigma(0)} \cong 1$$

for $|u| \ll 1$, and for a circular aperture $K_0 = (\pi/2)G_0^{\frac{1}{2}}$, then (38) becomes

$$\sigma_u = \frac{2}{\pi\delta}\left(\frac{2E_0L}{N_0}\right)^{-\frac{1}{2}} \text{std. BW.} \tag{39}$$

Thus at high signal-to-noise ratios the antenna dependence is

$$\sigma_u \approx \frac{1}{\delta}.$$

This dependence shows that the difference pattern angle sensitivity is of prime importance in determining the over-all system angle accuracy.

---

* The subscript Σ refers to sum pattern parameters.

The optimum system from the standpoint of angle estimation is one with δ and η_Σ equal to unity. As we pointed out before such a system would have unacceptably high sidelobes. The price of lower sidelobes is reduced sensitivity (Figure 15). The top curve shows the maximum relative directivity, $\eta_{max}(\Sigma)$, obtainable from a Taylor sum pattern.* Similarly, the N can be selected to maximize relative angle sensitivity, δ_{max}, for the asymptotic difference pattern (Figure 15).
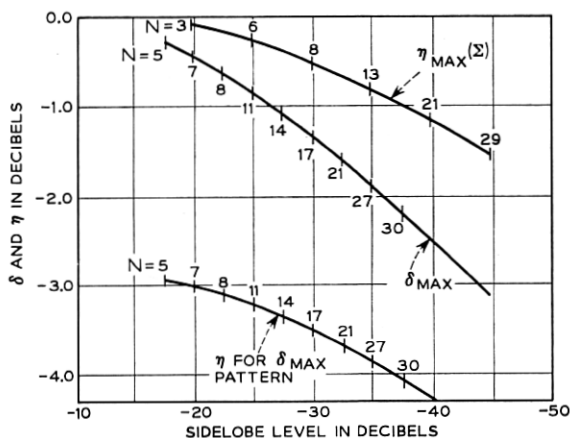

Fig. 15 — Relative directivity and angular sensitivity for maximum sensitivity pattern.

The relative directivity (η) of the δ_{max} pattern is shown at the bottom of Figure 15. Notice that it is 3 dB below the sum pattern relative directivity. Thus, to equalize the sidelobe clutter returns from the highest sidelobes in the sum and difference patterns, the difference pattern sidelobe level should be 3 dB greater than the sum pattern's sidelobe level. For example, if a sum pattern with -30 dB sidelobe level is chosen ($N = 8$) the difference pattern sidelobe level should be -27 dB, and δ_{max} is -1 dB when $N = 14$.

One of the major reasons for suppression of sidelobes is the presence of clutter. Although clutter can be a problem throughout the pattern it is often more prevalent at low angles. If clutter does not occur near the main beam it might be advantageous to choose a small value of N so that the sidelobes decay rapidly (Figure 9). If clutter is very bad it may be necessary to taper the transmitter illumination, too.

* Where N corresponds to $\bar{n}$ in Taylor's notation.

A second reason for suppression of sidelobes is the presence of active noise sources. These are the essence of the radio astronomy problem. For the radar problem they are jammers (electronic countermeasures). They generally are considered to be point sources which may appear anywhere in the pattern. Hence the requirement to minimize the maximum sidelobe level.

In selecting a difference pattern a major practical consideration is that the aperture function be realizable. Remember that the aperture function represents the resulting field on the face of the aperture (that is, after all ohmic losses and mutual couplings have been accounted for). Certainly one could not choose an aperture function with a lip or spike at the edge for use with a horn fed antenna or array. Even in an array of independent elements it usually is not desirable to let the edge excitation exceed the peak.

These considerations along with constraints of the system problem such as required accuracy, clutter, noise, and so on, influence the selection of sidelobe level and N.

V. SUMMARY

Full theoretical and design documentation has been given to a new two-parameter difference pattern. The salient features of the pattern are asymptotically equal sidelobes and near optimum angle sensitivity. The two parameters, A and N, give complete control of the sidelobe level and decay behavior. The difference pattern was designed to be compatible with monopulse systems using the Taylor sum beam illumination.

ACKNOWLEDGMENT

APPENDIX

Asymptotic Difference Pattern for a Line Source

The construction of an asymptotic difference pattern for a line source can be carried out in a manner similar to that described for the circular aperture. The equations for the line source difference pattern, which parallel those in the body of this report, are outlined here.

The line-source-to-pattern-function transform is a finite Fourier

transform.

$$F(u) = \int_{-\pi}^{\pi} g(x)e^{jux}\, dx \tag{40}$$

where $u = 2a/\lambda \sin \theta$, θ is measured from the normal, $2a$ is the length of the line source and x is normalized to π/a. Expand $g(x)$ in a sine series because an odd function is required

$$g(x) = \begin{cases} \displaystyle\sum_{l=0}^{N-1} B_l \sin \mu_l x; & -\pi \leq x \leq \pi \\ 0; & \text{elsewhere.} \end{cases} \tag{41}$$

A nonzero boundary value is again required for the truncated series. The eigenvalues must be $u_l = l + 1/2$. Now transforming the series by (40) and setting $u_l = l + 1/2$ yields

$$F(u) = 2j \sum_{l=0}^{N-1} B_l \frac{(-1)^l u \cos u_\pi}{(l + \frac{1}{2})^2 - u^2}. \tag{42}$$

The desired model function, $F_M(u)$ (see equations 12 and 14) is again described by its zeros.

The dilation factor is

$$\sigma = \frac{\mu_N}{Z_N} = \frac{N + \frac{1}{2}}{Z_N}. \tag{43}$$

The asymptotic function is given by the canonical product

$$F_a(u) = Cu \prod_{n=1}^{N-1} \left\{ 1 - \left(\frac{u}{\sigma Z_n}\right)^2 \right\} \prod_{l=N}^{\infty} \left\{ 1 - \left(\frac{u}{\mu_l}\right)^2 \right\} \tag{44}$$

where C is a constant.

The asymptotic difference pattern in closed form is:

$$F_a(u) = Cu \cos (\pi u) \left\{ \frac{\displaystyle\prod_{n=1}^{N-1} 1 - \left(\frac{u}{\sigma Z_n}\right)^2}{\displaystyle\prod_{l=0}^{N-1} 1 - \left(\frac{u}{\mu_l}\right)^2} \right\}. \tag{45}$$

The function may be expressed in series form by evaluating (45) at $u = \mu_m$ and setting it equal to (42) to find B_m. Evaluating the series (42) at $u = \mu_m$ gives

$$F(\mu_m) = \operatorname*{Lim}_{u \to \mu_m} F_a(u) = j\pi B_m . \tag{46}$$

Substituting $\mu_n = n + 1/2$, the coefficients are:

$$
B_m = \begin{cases} \dfrac{C}{2j} (-1)^m (m - \tfrac{1}{2})^2 \dfrac{\displaystyle\prod_{n=1}^{N-1}\left[1 - \left(\dfrac{m + \frac{1}{2}}{\sigma Z_n}\right)^2\right]}{\displaystyle\prod_{\substack{l=0 \\ l \neq m}}^{N-1}\left[1 - \left(\dfrac{m + \frac{1}{2}}{l + \frac{1}{2}}\right)^2\right]} ; & \\[4pt] & m = 0, 1, 2, \cdots, N - 1 \\ 0; & m = N, N + 1, \cdots \end{cases} \quad (47)
$$

As N is allowed to increase without bound it may be noticed that $\sigma \to 1$ from above and the zeros of $F_a(u)$ approach those of $F_M(u)$. Thus

$$
\lim_{N \to \infty} F_a(u) = F_M(u).
$$

For small N the values of B_m can be evaluated by hand by using the model function parameters from Figure 4.

REFERENCES

1. Taylor, T. T., "Design of Circular Apertures for Narrow Beamwidth and Low Sidelobes," IRE Trans. Antennas and Propagation, *AP-8* (January 1960), pp. 17–22.
2. Manasse, R., "Maximum-Angular Accuracy of Tracking a Radio Star by Lobe Comparison," IRE Trans. Antennas and Propagation, *AP-8* (January 1960), pp. 50–56.
3. Harrington, R. F., *Time-Harmonic Electromagnetic Fields,* New York: McGraw-Hill, 1961, pp. 110–112.
4. Plonsey, R., "Aperture Fields," IRE Trans. Antennas and Propagation, *AP-9* (November 1961), p. 577.
5. Hansen, R. C., *Microwave Scanning Antennas,* New York: Academic Press, 1964, vol. 1, pp. 5–11.
6. Ruze, J., "Circular Aperture Synthesis," IEEE Trans. Antennas and Propagation, *AP-12* (November 1964), pp. 691–694.
7. Price, O. R. and Hyneman, R. F., "Distribution Functions for Monopulse Antenna Difference Patterns," IRE Trans. Antennas and Propagation, *AP-8* (November 1960), pp. 567–576.
8. Dolph, C. L., "A Current Distribution for Broadside Arrays Which Optimizes the Relationship between Beamwidth and Sidelobe Level," *Proc. IRE, 34* (June 1946), pp. 335–348.
9. Sinclair, G. and Cairns, F. V., "Optimum Patterns for Arrays of Non-Isotropic Sources," IRE Trans. Antenna and Propagation, *AP-1* (February 1952), pp. 50–61.
10. Silver, S., *Microwave Antenna Theory and Design,* MIT Radiation Laboratory Series, vol. 12, New York: McGraw-Hill, 1949, p. 177.
11. Kinsey, R. R., "Monopulse Difference Slope and Gain Standards," IRE Trans. Antennas and Propagation, *AP-10* (May 1962), pp. 343–344.
12. Kirkpatrick, G. M., "Aperture Illuminations for Radar Angle-of-Arrival Measurements," IRE Trans. Aeronautical and Navigational Elec., *AE-9* (September 1953), pp. 20–27.
13. Rhodes, D. R., *Introduction to Monopulse,* New York: McGraw-Hill, 1959, p. 56.
14. McGinn, J. W., Jr., "Thermal Noise in Amplitude Comparison Monopulse Systems," IEEE Trans. Aerospace Elec. Syst., *AES-2,* (September 1966), pp. 550–556.